Static Liquefaction of Sands under Isotropically and K_0-Consolidated Undrained Triaxial Conditions

Xilin Lu[1] and Maosong Huang[2]

Abstract: By using the state-dependent strength criterion and dilatancy function, a state-dependent nonassociated elastoplasticity hardening model was proposed to unify modeling the constitutive relationships of sands with different initial void ratios. According to the second-order work theory, the criteria for predicting the potential instability and static liquefaction of sands were obtained. The proposed model and criteria were used to predict a series of isotropically consolidated and K_0-consolidated undrained triaxial tests. The results showed that the potentially unstable point and the onset of static liquefaction under undrained conditions coincided with the attainment of a deviatoric stress peak in very loose sand, whereas, with the decrease of the initial void ratio, the onset of static liquefaction fell behind the potential instability. When the sand specimen was dense enough, static liquefaction did not occur, although the stress state was located inside of the potentially unstable region. The potential instability and static liquefaction occurred before the effective stress reached the failure surface, and they were the precursors though not the results of the sand failures. **DOI: 10.1061/(ASCE)GT.1943-5606.0001206.** © *2014 American Society of Civil Engineers.*

Author keywords: Static liquefaction; Undrained triaxial tests; Critical state; Second-order work.

Introduction

The instability of soils that occurs before the peak failure often demonstrates as a localized or diffuse mode. The localized mode of instability appears in dense sand when loaded under drained condition, and it has been studied for a long time (Rudnicki and Rice 1975; Andrade and Borja 2006; Lu et al. 2011). For very loose sands, when monotonically loaded under an undrained condition, static liquefaction takes place; this kind of instability is different from the localized mode and keeps its homogeneous deformation. Static liquefaction is a typical and important characteristic of loosely compacted saturated soil, and it has been used in the stability analysis of saturated slope (Lade 1992; Ellison and Andrade 2009).

Static liquefaction has been studied experimentally by triaxial tests (Sladen et al. 1985; Lade and Pradel 1990; Yamamuro and Lade 1997; Doanh et al. 1997), plane-strain tests (Chu and Wanatowski 2008), and ring-shear tests (Liu et al. 2011). The influence of K_0 consolidation on static liquefaction was also studied experimentally (Fourie and Tshabalala 2005; Chu and Wanatowski 2008). Based on the summary of existing experimental results, the onset of static liquefaction instability could be determined by the instability line (Lade and Pradel 1990) or collapse surface (Sladen et al. 1985) in stress space. The experimental results (Daouadji et al. 2010; Wanatowski and Chu 2012) showed the main factors affecting instability are the stress state, drainage condition, loading mode, and material state. By summing up a series of experimental results, the undrained instability has been characterized by critical state theory (Rahman et al. 2011; Bedin et al. 2012). To describe the influence of the initial material state on instability, Yang (2002) expressed the instability line as a function of the current material state, and Rahman et al. (2011) defined the instability line as a function of the equivalent granular state parameter.

Compared with the experimental studies, there is lack of theoretical study on static liquefaction. Borja (2006) adopted the bifurcation theory to study the initiation of liquefaction instability in saturated soils. Andrade (2009) presented a practical mathematical framework for predicting the liquefaction instability, which has been shown to coincide with the loss of uniqueness of material response (Nova 1994). Buscarnera et al. (2011) studied diffuse instability by loss of controllability and derived the mathematical condition under different loading conditions. Based on the NorSand model (Jefferies 1993; Andrade and Ellison 2008), the critical hardening modulus corresponding to the onset of static liquefaction was obtained and adopted in numerical modeling of submarine slope (Ellison and Andrade 2009). In these works, static liquefaction was predicted to occur at the strain-softening stage; instability can also emerge within stable single-phase solids owing to the interaction between the solid matrix and fluid flow (Bardet and Iai 2002).

This paper proposes a model to calibrate the stress-strain relationships and study the onset of static liquefaction under different initial material states, consolidation states, and confining conditions. After a view of the critical state theory, a state-dependent Mohr-Coulomb elastoplasticity hardening model is proposed by using material state–dependent strength and stress dilatancy. Based on the second-order work criterion, the theoretical condition for static liquefaction is proposed and used to predict the results of isotropically consolidated and K_0-consolidated undrained triaxial compression tests. Finally, the influence of the initial material states of sands at the onset of static liquefaction is discussed.

[1]Associate Professor, Dept. of Geotechnical Engineering and Key Laboratory of Geotechnical and Underground Engineering of the Ministry of Education, Tongji Univ., Shanghai 200092, China; formerly, Visiting Associate Professor, Dept. of Mechanical and Civil Engineering, California Institute of Technology, Pasadena, CA 91125 (corresponding author). E-mail: xilinlu@tongji.edu.cn

[2]Professor and Chair, Dept. of Geotechnical Engineering and Key Laboratory of Geotechnical and Underground Engineering of the Ministry of Education, Tongji Univ., Shanghai 200092, China.

Note. This manuscript was submitted on November 10, 2012; approved on September 2, 2014; published online on September 29, 2014. Discussion period open until March 1, 2015; separate discussions must be submitted for individual papers. This paper is part of the ***Journal of Geotechnical and Geoenvironmental Engineering***, © ASCE, ISSN 1090-0241/04014087(9)/$25.00.

State-Dependent Elastoplasticity Model: Critical State Theory

The state parameter ψ (Been and Jefferies 1985), which represents the difference of current void ratio e and the void ratio e_c at the critical state in the same mean pressure, can be used to determine the state of soil

$$\psi = e - e_c \tag{1}$$

The void ratio e_c at the critical state line depends on the mean pressure; it can be defined by (Yang and Li 2004)

$$e_c = e_{c0} - \lambda_c \left(\frac{p}{p_{at}}\right)^{\xi} \tag{2}$$

where $p_{at} = 101.3$ kPa = atmospheric pressure; and e_{c0}, λ_c, and ξ = material parameters that are used to determine the critical state line in the e, p-plane.

In Fig. 1, the state parameter ψ clearly shows the state of the sand; a negative value indicates dilative state and a positive value indicates contractive state. It should be noted that, in an undrained case, the total volumetric strain always keeps constant, and the attainment of the state parameter to the critical state is caused by the changes in the effective mean pressure.

State-Dependent Mohr-Coulomb Hardening Model

Considering the theoretical prediction of the onset of static liquefaction relies on the constitutive relationships, a sophisticated model needs to be developed to capture the instability characteristic of the sands with different initial material states. Here, for simplicity, the constitutive model is proposed on the basis of the widely used elastoplastic Mohr-Coulomb hardening model. The yield function is

$$F = q - Mp' = 0 \tag{3}$$

where $p' = \sigma_{ii}/3 - u$; $q = \sqrt{3J_2} = \sqrt{3s'_{ij}s'_{ij}/2}$; $s'_{ij} = \boldsymbol{\sigma}'_{ij} - \delta_{ij}p'$; $\boldsymbol{\sigma}'_{ij} = \boldsymbol{\sigma}_{ij} - u$; u = pore-water pressure; and δ_{ij} = Kronecker delta.

The evolution of M is assumed to follow the hyperbolic law (Pietruszczak and Stolle 1987; Huang et al. 2010)

$$M = M_p \frac{\varepsilon_s^p}{A + \varepsilon_s^p} \tag{4}$$

where the equivalent plastic shear strain $\varepsilon_s^p = \sqrt{2e_{ij}e_{ij}/3}$; $e_{ij} = \boldsymbol{\varepsilon}_{ij} - \delta_{ij}\varepsilon_{ii}/3$; and A = fitting parameter. The peak value of stress ratio

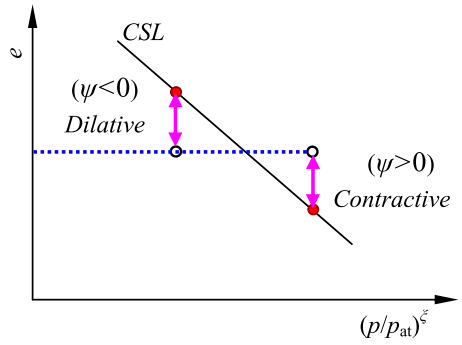

Fig. 1. Critical state line in e-$(p/p_{at})^{\xi}$ plane

M_p is assumed to be state-dependent and can be expressed as (Manzari and Dafalias 1997)

$$M_p = M_{cs}\exp\left(-n^b\psi\right) \tag{5}$$

The plastic dilatancy is

$$D = \frac{d\varepsilon_v^p}{d\varepsilon_s^p} \tag{6}$$

A framework is needed to define a unique relationship between the stress ratio and the dilatancy. To capture the influence of the material state, the state parameter should be included in the stress-dilatancy function, and it could be formulated as (Li and Dafalias 2000; Gajo and Wood 2001)

$$D = A_d[M_d - M] = A_d\left[M_{cs}\exp\left(n^d\psi\right) - M\right] \tag{7}$$

where $A_d = d_0/M_{cs}$; and n^d and d_0 = material parameters.

For simplicity, here A_d is assumed to be 1, and then Eq. (7) is the same for the dilatancy function in the Cam-clay model and can be formulated equivalently by using the plastic potential function

$$G = q + M_d p' \ln\frac{p'}{p_0} = 0 \tag{8}$$

From Eqs. (3) and (8), the gradient of yield function and plastic potential function to p' and q are

$$\begin{aligned} \frac{\partial F}{\partial p'} &= -M \\ \frac{\partial F}{\partial q} &= 1 \end{aligned} \tag{9}$$

$$\begin{aligned} \frac{\partial Q}{\partial p'} &= M_d - \frac{q}{p'} \\ \frac{\partial Q}{\partial q} &= 1 \end{aligned} \tag{10}$$

The rate form of elastoplasticity constitutive relationship is

$$\dot{\sigma}_{ij} = \mathbf{D}^{ep}_{ijkl}\dot{\varepsilon}_{kl} \tag{11}$$

where the elastoplastic modulus is

$$\mathbf{D}^{ep}_{ijkl} = \mathbf{D}^{e}_{ijkl} - \mathbf{D}^{p}_{ijkl} = \left(K - \frac{2}{3}G\right)\delta_{ij}\delta_{kl} + G\left(\delta_{ik}\delta_{jl} + \delta_{il}\delta_{jk}\right) - \frac{D^e_{ijmn}\dfrac{\partial Q}{\partial \sigma'_{mn}}\left(\dfrac{\partial F}{\partial \sigma'_{pq}}\right)^T D^e_{pqkl}}{\left(\dfrac{\partial F}{\partial \sigma'_{uv}}\right)^T D^e_{uvst}\dfrac{\partial Q}{\partial \sigma'_{st}} + H_p} \tag{12}$$

The hardening modulus is

$$H_p = -\frac{\partial F}{\partial M}\frac{\partial M}{\partial \varepsilon_s^p} = p' M_p \frac{A}{\left(A + \varepsilon_{ep}\right)^2} \tag{13}$$

The bulk modulus K and shear modulus G are related to the state of sand and can be expressed by the current void ratio e as (Richart et al. 1970)

$$K = \frac{2(1+\nu)}{3(1-2\nu)}G$$
$$G = G_0 p_{at}\frac{(2.97-e)^2}{1+e}\sqrt{\frac{p'}{p_{at}}} \tag{14}$$

where G_0 = regression constant of the elastic shear modulus; and ν = Poisson's ratio.

p-q Form under Triaxial Condition

To simulate the stress-strain relationship of soil under the triaxial condition conveniently, Eq. (11) is rewritten into p-q form as

$$\dot{p}' = K\dot{\varepsilon}_v^e = K\left(\dot{\varepsilon}_v - \dot{\lambda}\frac{\partial Q}{\partial p'}\right)$$
$$\dot{q} = 3G\dot{\varepsilon}_s^e = 3G\left(\dot{\varepsilon}_s - \dot{\lambda}\frac{\partial Q}{\partial q}\right) \tag{15}$$

where $\varepsilon_s = 2(\varepsilon_a - \varepsilon_r)/3$; $\varepsilon_v = 2\varepsilon_a + \varepsilon_r$; $p' = (\sigma'_a + 2\sigma'_r)/3$; $q = \sigma'_a - \sigma'_r$; ε_a and ε_r = axial and radial strains; and σ'_a and σ'_r = axial and radial effective stresses.

The plastic multiplier could be obtained from the consistency condition and can be expressed as

$$\dot{\lambda} = \frac{K\frac{\partial F}{\partial p'}\dot{\varepsilon}_v + 3G\frac{\partial F}{\partial q}\dot{\varepsilon}_s}{H_p + K\frac{\partial F}{\partial p'}\frac{\partial Q}{\partial p'} + 3G\frac{\partial F}{\partial q}\frac{\partial Q}{\partial q}} \tag{16}$$

Using Eqs. (9) and (10), Eq. (16) becomes

$$\dot{\lambda} = \frac{-KM\dot{\varepsilon}_v + 3G\dot{\varepsilon}_s}{H_p + KM(M - M_d) + 3G} \tag{17}$$

The deviatoric and volumetric plastic strain rates are

$$\dot{\varepsilon}_v^p = \dot{\lambda}\frac{\partial Q}{\partial p'} = \dot{\lambda}M_d\left(\ln\frac{p'}{p_0} + 1\right) = \dot{\lambda}(M_d - M)$$
$$\dot{\varepsilon}_s^p = \dot{\lambda}\frac{\partial Q}{\partial q} = \dot{\lambda} \tag{18}$$

By inserting Eq. (18) into Eq. (15), one gets

$$\dot{p}' = K\left[\dot{\varepsilon}_v - \dot{\lambda}(M_d - M)\right]$$
$$\dot{q} = 3G\left(\dot{\varepsilon}_s - \dot{\lambda}\right) \tag{19}$$

After arrangement, the rate form of the constitutive relationship is

$$\begin{Bmatrix}\dot{p}'\\ \dot{q}\end{Bmatrix} = \mathbf{D}_{pq}^{ep}\begin{Bmatrix}\dot{\varepsilon}_v\\ \dot{\varepsilon}_s\end{Bmatrix} \tag{20}$$

where

$$\mathbf{D}_{pq}^{ep} = \begin{bmatrix} K + \frac{K^2M(M_d - M)}{H_p + KM(M - M_d) + 3G} & \frac{-3KG(M_d - M)}{H_p + KM(M - M_d) + 3G} \\ \frac{3KGM}{H_p + KM(M - M_d) + 3G} & 3G - \frac{9G^2}{H_p + KM(M - M_d) + 3G} \end{bmatrix}$$

K_0-Consolidated Condition

When the state-dependent Mohr-Coulomb hardening model was used to simulate the K_0-consolidated undrained triaxial tests, the evolution of M needed to be changed as

$$M = M_0 + (M_p - M_0)\frac{\varepsilon_s^p}{A + \varepsilon_s^p} \tag{21}$$

where M_0 = stress ratio after K_0 consolidation.

The hardening modulus under K_0-consolidated condition becomes

$$H_p = p'(M_p - M_0)\frac{A}{(A + \varepsilon_{ep})^2} \tag{22}$$

It should be noted that the proposed model is different from the standard Mohr-Coulomb hardening models, which treat soils in different initial states as different materials. By using the state parameter to calibrate the influence of void ratio and mean stress on the peak stress ratio and stress dilatancy, the proposed model could unify modeling the constitutive relationship of sands under different initial void ratios, confining stresses, and consolidation conditions. This model takes advantage of the other critical state models (Jefferies 1993; Wood and Belkheir 1994; Li et al. 1999; Wan and Guo 2004; Andrade and Ellison 2008), but it is quite simple and could be applied easily in engineering.

Criteria of Static Liquefaction

In the conventional plasticity theory, instability is assumed to occur when the stress state reaches the failure surface. However, the occurrence of static liquefaction induces the unstable behavior of saturated soils before the failure stress state is reached (Daouadji et al. 2010), and the shear stress decreases after the onset of static liquefaction. The instability line often was used to judge the stable or unstable behavior of the soil, and it is obtained generally from experimental results. The instability condition of soil could be investigated theoretically on the basis of a second-order work criterion, which has been used to check the onset of instability or strain softening by Valanis (1985) and Chu et al. (1992). Whether the second-order work criterion is sufficient for instability or not has been studied (Lade et al. 1987, 1988; Chu et al. 1993; Chu and Wanatowski 2009). Here, the second-order work criterion was used to study the static liquefaction of sands with different initial void ratios under isotropically consolidated and K_0-consolidated

undrained triaxial condition, and the typical stress paths studied are shown in Fig. 2.

In an infinitesimal deformation condition, according to the second-order work criterion, the stability of material requires

$$d^2w = d\tilde{\boldsymbol{\sigma}}' : d\tilde{\boldsymbol{\varepsilon}} > 0, \quad \forall \|d\tilde{\boldsymbol{\varepsilon}}\| \neq 0 \tag{23}$$

where d^2w = second-order work; $d\tilde{\boldsymbol{\sigma}}'$ = effective stress increment; and $d\tilde{\boldsymbol{\varepsilon}}$ = corresponding strain increment.

It could be inferred that, if there exists a loading path that results in the violation of Eq. (23), the material becomes potentially unstable, so the condition of the potential instability is

$$d^2w = d\tilde{\boldsymbol{\sigma}}' : d\tilde{\boldsymbol{\varepsilon}} \leq 0, \quad \exists \|d\tilde{\boldsymbol{\varepsilon}}\| \neq 0 \tag{24}$$

After inserting Eq. (11) or Eq. (20), one gets

$$d\tilde{\boldsymbol{\varepsilon}} : \mathbf{D}^{ep} : d\tilde{\boldsymbol{\varepsilon}} \leq 0, \quad \exists \|d\tilde{\boldsymbol{\varepsilon}}\| \neq 0 \tag{25}$$

Eq. (25) implies the vanishing determinant value of the symmetric part

$$\det\left(\mathbf{D}^{ep}_{\text{sys}}\right) \leq 0 \tag{26}$$

When under a triaxial condition, the criterion of Eq. (26) becomes

$$\det\left[\left(\mathbf{D}^{ep}_{pq}\right)_{\text{sys}}\right] \leq 0 \tag{27}$$

Eq. (24) also could be expressed by replacing the strain increment with stress rate

$$d\tilde{\boldsymbol{\sigma}}' : \mathbf{C}^{ep} : d\tilde{\boldsymbol{\sigma}}' \leq 0, \quad \exists \left\|d\tilde{\boldsymbol{\sigma}}'\right\| \neq 0 \tag{28}$$

where $\mathbf{C}^{ep}$ = inversion of $\mathbf{D}^{ep}$. The determinant of the symmetric part of both tensors goes to zero simultaneously (Prunier et al. 2009), so the analysis based on both tensors would give the same results.

It should be noted that Eqs. (26) and (27) are necessary but insufficient conditions of Eq. (25). Once Eq. (26) is satisfied, the soil becomes potentially unstable and the stability depends on the stress increment. It could be inferred that the soil could stay stable as long as the stress increment is not along the unstable stress path, even if the soil is potentially unstable. Also, it should be noted that the negative value of the second-order work is necessary but insufficient

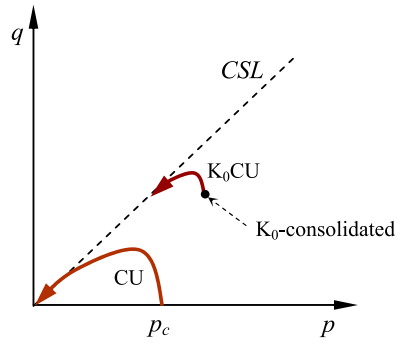

Fig. 2. Stress path analyzed (CU = consolidated undrained compression triaxial test; K_0CU = K_0-consolidated undrained compression triaxial test; CSL = critical state line)

for the static liquefaction (Chu and Leong 2001), and the additional conditions are (Lade 1992)

$$\frac{\partial F}{\partial \sigma_{ij}} \cdot \delta_{ij} < 0$$
$$\frac{\partial Q}{\partial \sigma_{ij}} \cdot \delta_{ij} > 0 \tag{29}$$

By substituting Eqs. (3) and (8) into Eq. (29), the first inequality is satisfied, and the second inequality requires $M_d - M > 0$. It can be concluded that the tendency of volumetric compression of the soil under undrained conditions combined with the violation of second-order work yield the complete condition for static liquefaction to occur.

Experimental Predictions

To assess the proposed model and the criteria of static liquefaction, experimental results (e.g., undrained triaxial test) are required for validation. There are two kinds of loading modes for undrained triaxial tests: (1) load-controlled loading mode, and (2) deformation-controlled loading mode. In load-controlled triaxial tests, instability occurs along with the sudden increase of strain rate, whereas in deformation-controlled tests, prefailure strain softening takes places under the same other conditions (Chu and Leong 2001). Although both phenomena are different, the mechanism that governs the onset of instability is the same and could be predicted by the same criteria (Chu and Leong 2001; Chu and Wanatowski 2009). Because this study focused on the onset of static liquefaction instability and the soil behavior at postpeak stage is beyond the study's scope, only the deformation-controlled triaxial tests were analyzed.

Isotropically Consolidated Undrained Triaxial Tests

The proposed constitutive model and the instability criteria were used to predict the results of the isotropically consolidated undrained triaxial tests of Doanh et al. (1997). The specimen, which was 70 mm in diameter and 70 mm in height, was made of Hostun RF sand with minimum void ratio $e_{\min} = 0.648$ and maximum void ratio $e_{\max} = 1.041$. The void ratios of the specimen after isotropical consolidation were 0.883, 0.875, and 0.854. The initial effective consolidation pressures of the tests were 100, 200, and 300 kPa.

The elastic parameter G_0 is a regression constant and could be determined by fitting a series of independent small-strain test data (e.g., from bender element tests) using Eq. (14); Poisson's ratio ν could be determined by Eq. (14) when the bulk modulus was known. The parameter M_{cs} and parameters λ_c, e_{c0}, and ξ were determined by fitting the experimental data of the stress ratio and e-p data at the critical state. The obtained e_c-p curve of Hostun RF sand (Doanh and Ibraim 2000) is shown in Fig. 3. The n_b could be determined by Eq. (5) from the measured data of ψ and M at the phase-transformation state, n_d could be determined by Eq. (7) from the measured data of ψ and M at the drained peak stress state, and d_0 could be determined by the ε_v-ε_q curve from the drained triaxial test. A fitting parameter A could be obtained by fitting the stress-strain relationships.

After all the material parameters were calibrated (listed in Table 1), the behavior of the specimen was predicted by deformation-controlled loading. As shown in Fig. 4, the predicted effective stress path under undrained loading process compared very well with the experiments. The predicted effective stress-strain relationship and pore-water pressure are shown in Fig. 5; the deviatoric shear stress rapidly increased to the peak, and then decreased along with the

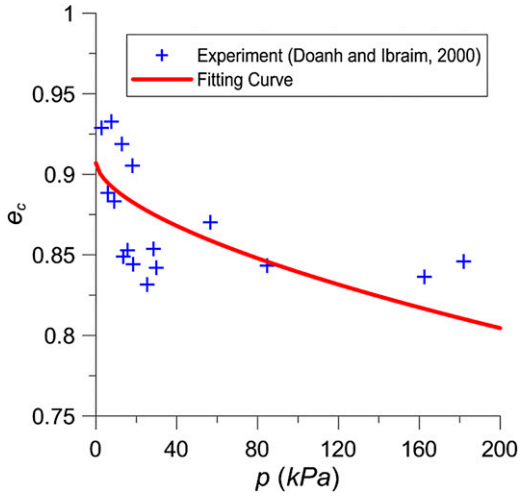

Fig. 3. The e_c-p curve at critical state (experimental data from Doanh and Ibraim 2000)

Table 1. Material Parameters Used in the Simulation [Experimental Data from Doanh et al. (1997) and Chu and Wanatowski (2008)]

Material parameters	Istropically consolidated undrained triaxial tests	K_0-consolidated undrained triaxial tests
G_0	125	30
ν	0.15	0.05
M_{cs}	1.0	1.35
λ_c	0.078	0.098
e_{c0}	0.907	0.972
ξ	0.6	0.4
n_b	1.1	1.1
n_d	3.5	3.5
d_0	0.88	0.88
A	0.001	0.003

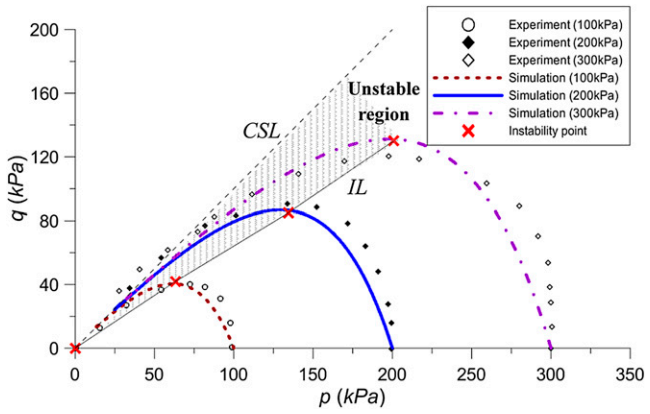

Fig. 4. Stress path of isotropically consolidated undrained triaxial test (experimental data from Doanh et al. 1997)

continuous increase in pore-water pressure. During the loading process, the determinant of the symmetric elastoplastic modulus tensor and second-order work were calculated. As shown in Fig. 6, both values vanished simultaneously at the peak of the deviatoric stress, which indicates that the static liquefaction started when the soil entered into the potentially unstable state. The evolution of the

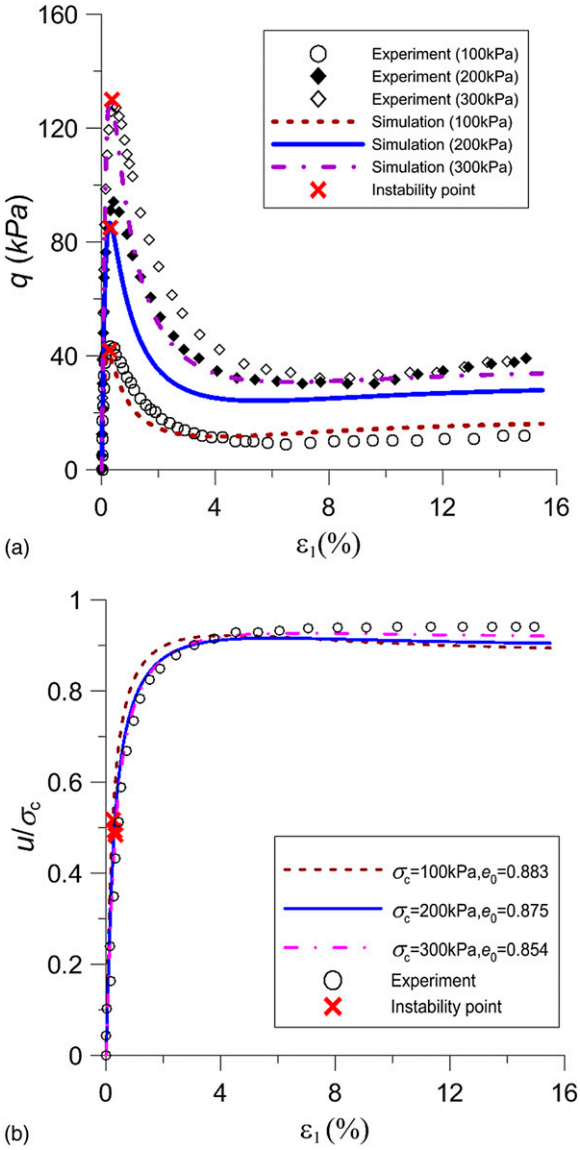

Fig. 5. Model prediction (experimental data from Doanh et al. 1997): (a) deviatoric stress, major principal strain; (b) normalized pore pressure, major principal strain

hardening modulus H_p is shown in Fig. 7; the static liquefaction occurred at the hardening stage of the soil. The difference between these results and those of Andrade (2009), in which static liquefaction occurred at the softening regime of the soil, is due to the adoption of a different kind of constitutive model.

K_0-Consolidated Undrained Triaxial Tests

The proposed constitutive model and instability criteria were used to predict the results of the K_0-consolidated undrained triaxial tests of Chu and Wanatowski (2008). The specimen was made of Singapore marine-dredged silica sand with mean grain size 0.30–0.35 mm, uniformity coefficient 2.0, specific gravity 2.6, maximum void ratio 0.916, and minimum void ratio 0.533. The specimen was 100 mm in diameter and 190 mm in height. After K_0 consolidation, the void ratios of the specimens were 0.844, 0.881, 0.899, and 0.922.

As shown in Fig. 8, the e_c-p curve at the critical state was calibrated from the experimental results of Chu et al. (2003) in the same sands.

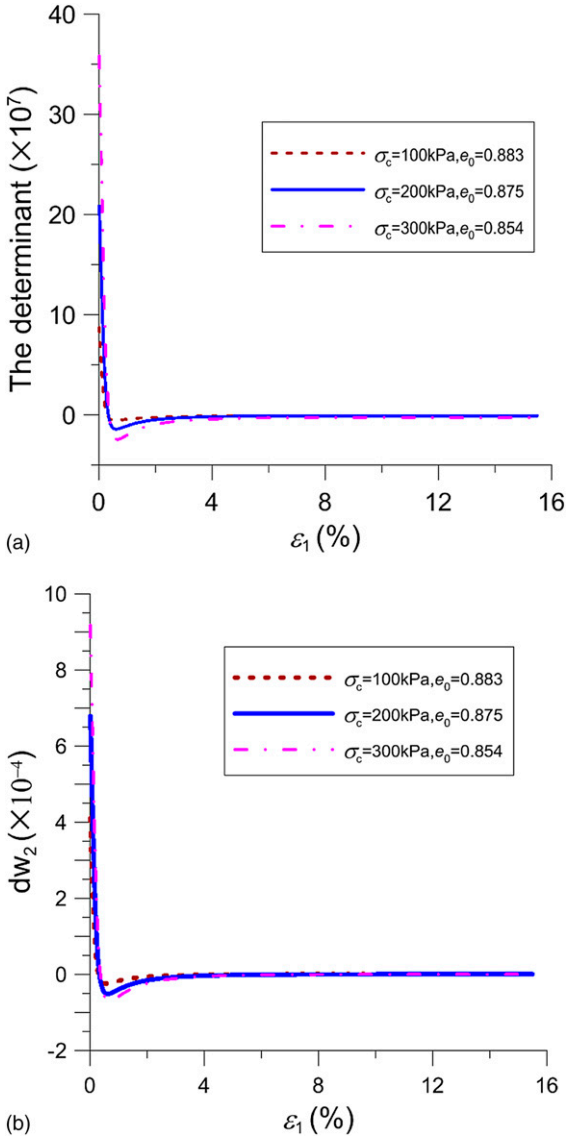

Fig. 6. Evolution of (a) determinant of the symmetric part of the elastoplastic modulus tensor and (b) second-order work

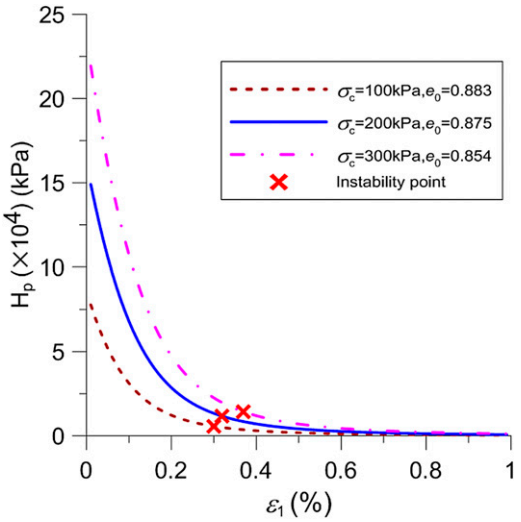

Fig. 7. Evolution of hardening modulus

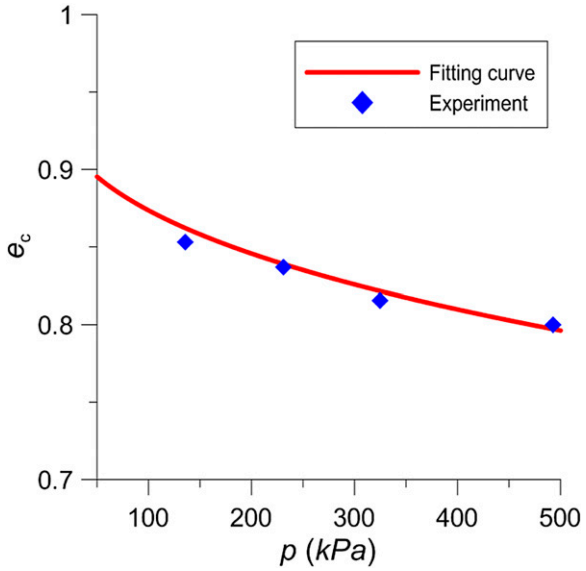

Fig. 8. The e_c-p curve at critical state (experimental data from Chu et al. 2003)

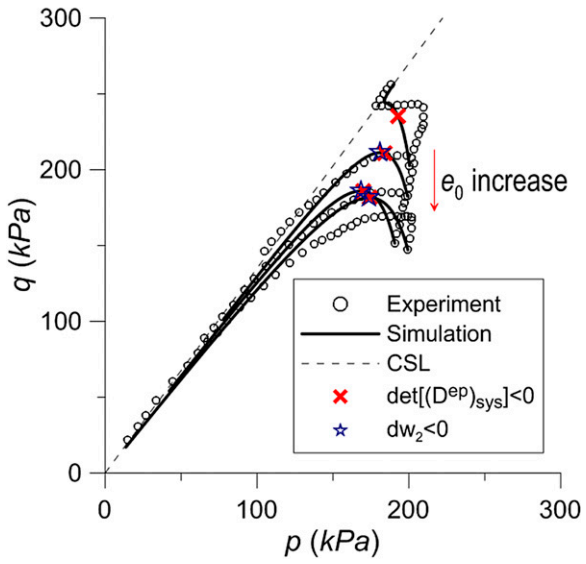

Fig. 9. Stress path of K_0-consolidated undrained triaxial test (experimental data from Chu and Wanatowski 2008)

By using the material parameters in Table 1, the mechanical behavior of the K_0-consolidated saturated sands under undrained loading were obtained. The predicted effective stress path is shown in Fig. 9. For relatively loose sand ($e_0 = 0.881, 0.899, 0.922$), the undrained loading induced the reduction of the mean pressure and the increase of deviatoric shear stress; after the attainment of its peak value, the deviatoric shear stress decreased. The test of the densest sands ($e_0 = 0.844$) showed the same trend as with the other three tests at the beginning of the loading stage; when the stress state approached the steady state, the deviatoric shear stress reversed and kept increasing, owing to the phase transition (Ishihara 1993). The predicted stress-strain relationship and pore-water pressure are shown in Figs. 10(a and b). The deviatoric shear stress first increased and then

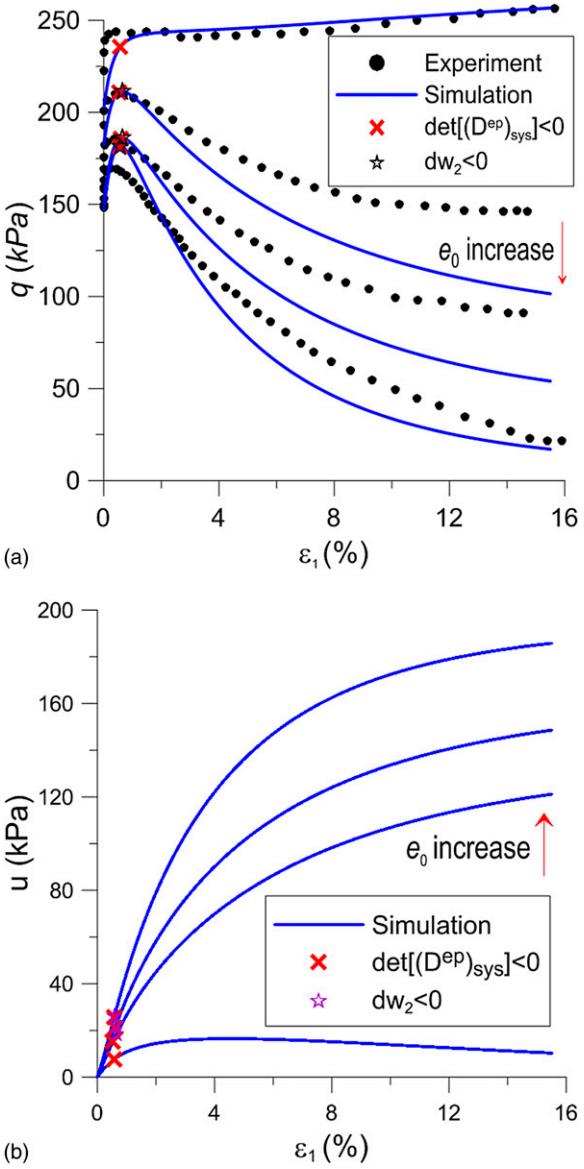

Fig. 10. Model prediction (experimental data after Chu and Wanatowski 2008): (a) stress-strain relationship; (b) evolution of pore-water pressure

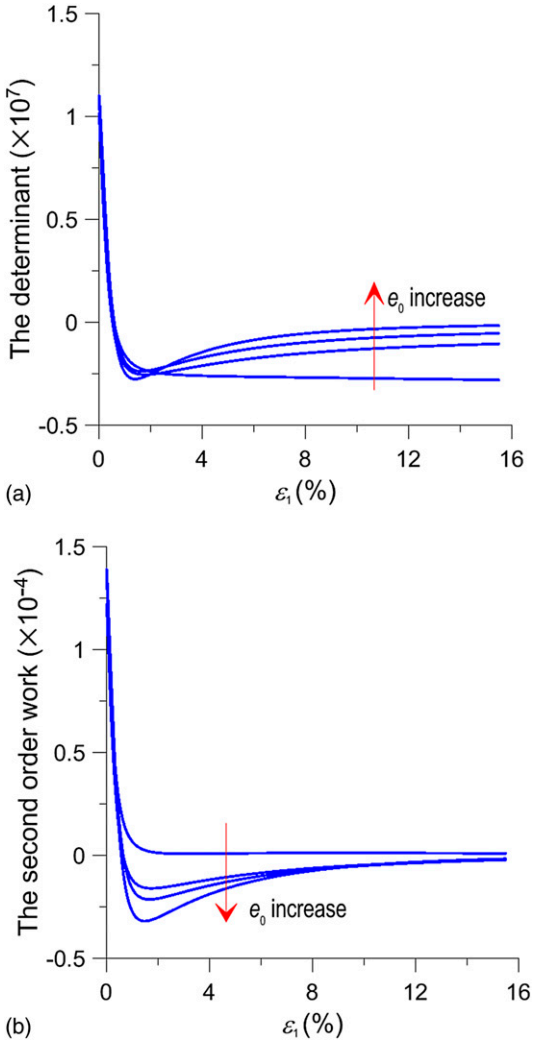

Fig. 11. Evolution of (a) determinant of the symmetric part of the elastoplastic modulus tensor; and (b) second-order work

decreased with the applied strain in three relatively loose sand specimens; in the case of the densest sand specimen, the deviatoric shear stress kept increasing and the peak value never appeared. As shown in Fig. 10(b), the pore-water pressure increased to a constant value when the sands reached the steady state. Compared with the three looser specimens, less pore-water pressure developed in the relatively dense specimen.

The determinant of the symmetric part of elastoplastic modulus tensor [Fig. 11(a)] and the second-order work [Fig. 11(b)] were calculated; all the determinants became negative when loading to approximately 0.6% of axial strain, which indicates that all the samples entered into potentially unstable states. As shown in Fig. 11(b), the second-order work for the densest specimen ($e_0 = 0.844$) never turned negative, which indicates that static liquefaction would not occur. As shown in Fig. 12, although the stresses showed a descending trend after the onset of static liquefaction, both the potentially unstable points and static liquefaction point occurred at the hardening regime. To clarify the

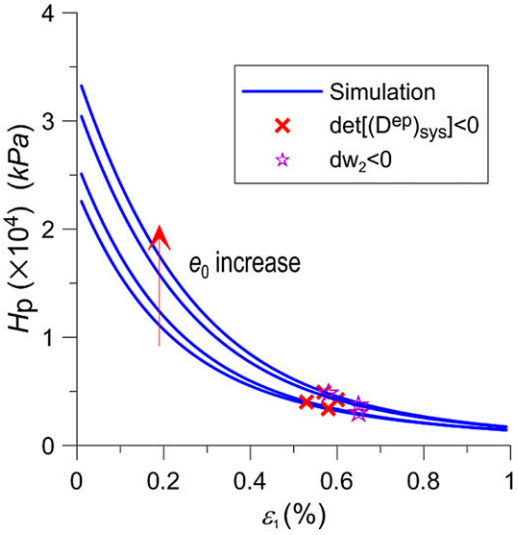

Fig. 12. Evolution of hardening modulus

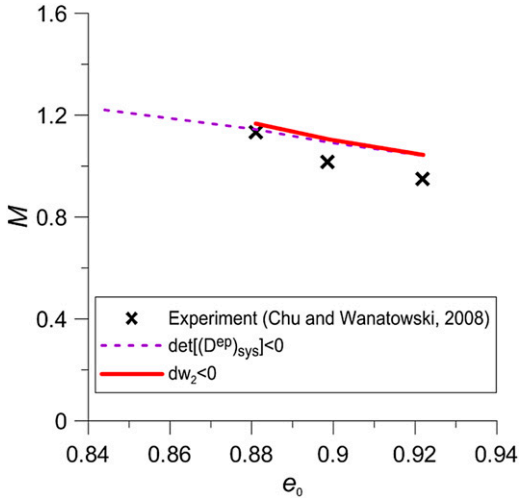

Fig. 13. Influence of the initial void ratio on the stress ratio at the onset of static liquefaction

influence of the initial material state on the shear strength at static liquefaction, the relationship between the initial void ratio and the stress ratio at the instability point is shown in Fig. 13. The stress ratio at the instability point decreased along with the increase of initial void ratio, and the predicted results agreed with the experimental results.

Conclusions

A state-dependent nonassociated Mohr-Coulomb hardening elastoplasticity model and second-order work criterion were proposed to study the static liquefaction under the undrained triaxial condition. The vanishing value of the determinant of the symmetric part of the elastoplastic modulus tensor was used to predict the potentially unstable state of soils, and the sign change in second-order work denoted the onset of static liquefaction. The static liquefaction initiated only when the undrained stress path occurred along with the potentially unstable stress path, or when the soil stayed stable even the stress state was located in the potentially unstable region.

The proposed model and instability criteria were used to analyze a series of isotropically consolidated and K_0-consolidated undrained triaxial tests. The results showed that static liquefaction is prone to occur in loose sands, although when the sand is dense enough, it would be prevented by the tendency of dilatancy even if the state of sands becomes potentially unstable. The static liquefaction occurred at the hardening regime of sands before the plastic limit failure criterion was reached; its occurrence induced the drop of shear resistance and the increase of pore-water pressure.

Acknowledgments

The financial support given by the National Basic Research Program of China (grant 2012CB719803), National Science Foundation of China (NSFC grant 11372228), and Shanghai Municipal Science and Technology Commission (grant 13ZR1443800) are gratefully acknowledged. The first author also extends his thanks to Professor José E Andrade at the California Institute of Technology for his help in doing the research. The authors are grateful to the anonymous reviewers for their helpful comments and suggestions.

Notation

The following symbols are used in this paper:

A = fitting parameter of hardening rule;
A_d = parameter of plastic potential function;
D = dilatancy function;
$\mathbf{D}^e_{ijkl}$, $\mathbf{D}^e$ = elastic modulus tensor;
$\mathbf{D}^{ep}_{ijkl}$, $\mathbf{D}^{ep}$ = elastoplastic modulus tensor;
$(\mathbf{D}^{ep})_{\text{sys}}$ = symmetric part of elastoplastic modulus tensor;
$\mathbf{D}^p_{ijkl}$, $\mathbf{D}^p$ = plastic modulus tensor;
$d\tilde{\boldsymbol{\varepsilon}}$ = arbitrary strain increment;
$d\tilde{\boldsymbol{\sigma}}'$ = arbitrary effective stress increment;
d_0 = parameter of plastic potential function;
E = elastic modulus;
e = void ratio;
e_c = void ratio at critical state;
e_{c0} = critical void ratio at zero pressure;
e_{ij} = deviatoric strain;
F = yield function;
G = pressure-dependent shear modulus;
G_0 = regression constant of elastic shear modulus;
H = hardening modulus;
J_2 = second stress invariant;
K = bulk elastic modulus;
K_0 = coefficient of stress after consolidation;
M = stress ratio;
M_{cs} = stress ratio at critical state;
M_d = dilatancy stress ratio;
M_f = peak stress ratio;
M_0 = stress ratio after K_0 consolidation;
n^b = parameter for the dilatancy description;
n^d = parameter for the peak stress ratio;
p' = mean stress;
p_{at} = atmospheric pressure;
Q = plastic potential;
q = equivalent shear stress;
s'_{ij} = effective deviatoric stress;
δ_{ij} = Kronecker delta;
ε_a = axial strain;
$\boldsymbol{\varepsilon}_{ij}$ = strain tensor;
ε_r = radial strain;
ε_s = equivalent strain;
$\dot{\varepsilon}_s$ = equivalent shear strain rate;
ε_v = volumetric strain;
$\dot{\varepsilon}_v$ = equivalent volumetric strain rate;
$\dot{\varepsilon}^e_s$ = elastic equivalent shear strain rate;
$\dot{\varepsilon}^e_v$ = elastic equivalent volumetric strain rate;
ε^p_s = equivalent plastic strain;
λ = plastic multiplier;
λ_c = critical state line material constant;
ν = Poisson's ratio;
ξ = critical state line material constant;
σ'_a = effective axial stress;
$\boldsymbol{\sigma}_{ij}$, $\boldsymbol{\sigma}'_{ij}$ = total stress and effective stress tensors;
σ'_r = effective radial stress; and
ψ = material state parameter.

References

Andrade, J. E. (2009). "A predictive framework for liquefaction instability." *Géotechnique*, 59(8), 673–682.

Andrade, J. E., and Borja, R. I. (2006). "Capturing strain localization in dense sands with random density." *Int. J. Numer. Methods Eng.*, 67(11), 1531–1564.

Andrade, J. E., and Ellison, K. C. (2008). "Evaluation of a predictive constitutive model for sands." *J. Geotech. Geoenviron. Eng.*, 10.1061/(ASCE)1090-0241(2008)134:12(1825), 1825–1828.

Bardet, J. P., and Iai, S. (2002). "Axisymmetric instability of fluid saturated pervious cylinders." *J. Appl. Mech.*, 69(6), 717–723.

Bedin, J., Schnaid, F., Da Fonseca, A. V., and Costa Filho, L. De M. (2012). "Gold tailings liquefaction under critical state soil mechanics." *Géotechnique*, 62(3), 263–267.

Been, K., and Jefferies, M. G. (1985). "A state parameter for sands." *Géotechnique*, 35(2), 99–112.

Borja, R. I. (2006). "Condition for liquefaction instability in fluid-saturated granular soils." *Acta Geotech.*, 1(4), 211–224.

Buscarnera, G., Dattola, G., and di Prisco, C. (2011). "Controllability, uniqueness and existence of the incremental response: A mathematical criterion for elastoplastic constitutive laws." *Int. J. Solids Struct.*, 48(13), 1867–1878.

Chu, J., and Leong, W. K. (2001). "Pre-failure strain softening and pre-failure instability of sand: A comparative study." *Géotechnique*, 51(4), 311–321.

Chu, J., Leroueil, S., and Leong, W. K. (2003). "Unstable behaviour of sand and its implication for slope instability." *Can. Geotech. J.*, 40(5), 873–885.

Chu, J., Lo, S.-C. R., and Lee, I. K. (1992). "Strain-softening behavior of granular soil in strain-path testing." *J. Geotech. Engrg.*, 10.1061/(ASCE)0733-9410(1992)118:2(191), 191–208.

Chu, J., Lo, S.-C. R., and Lee, I. K. (1993). "Instability of granular soils under strain path testing." *J. Geotech. Engrg.*, 10.1061/(ASCE)0733-9410(1993)119:5(874), 874–892.

Chu, J., and Wanatowski, D. (2008). "Instability conditions of loose sand in plane strain." *J. Geotech. Geoenviron. Eng.*, 10.1061/(ASCE)1090-0241(2008)134:1(136), 136–142.

Chu, J., and Wanatowski, D. (2009). "Effect of loading mode on strain softening and instability behavior of sand in plane-strain tests." *J. Geotech. Geoenviron. Eng.*, 10.1061/(ASCE)1090-0241(2009)135:1(108), 108–120.

Daouadji, A., AlGali, H., Darve, F., and Zeghloul, A. (2010). "Instability in granular materials: Experimental evidence of diffuse mode of failure for loose sands." *J. Eng. Mech.*, 10.1061/(ASCE)EM.1943-7889.0000101, 575–588.

Doanh, T., and Ibraim, E. (2000). "Minimum undrained strength of Hostun RF sand." *Géotechnique*, 50(4), 377–392.

Doanh, T., Ibraim, E., and Matiotti, R. (1997). "Undrained instability of very loose Hostun sand in triaxial compression and extension. Part 1: Experimental observations." *Mech. Cohes. Frict. Mater.*, 2(1), 47–70.

Ellison, K. C., and Andrade, J. E. (2009). "Liquefaction mapping in finite-element simulations." *J. Geotech. Geoenviron. Eng.*, 10.1061/(ASCE)GT.1943-5606.0000122, 1693–1701.

Fourie, A. B., and Tshabalala, L. (2005). "Initiation of static liquefaction and the role of K_0 consolidation." *Can. Geotech. J.*, 42(3), 892–906.

Gajo, A., and Wood, D. M. (2001). "A new approach to anisotropic, bounding surface plasticity: General formulation and simulations of natural and reconstituted clay behaviour." *Int. J. Numer. Anal. Methods Geomech.*, 25(3), 207–241.

Huang, M. S., Lu, X. L., and Qian, J. G. (2010). "Non-coaxial elasto-plasticity model and bifurcation prediction of shear banding in sands." *Int. J. Numer. Anal. Methods Geomech.*, 34(9), 906–919.

Ishihara, K. (1993). "Liquefaction and flow failure during earthquakes." *Géotechnique*, 43(3), 351–415.

Jefferies, M. G. (1993). "Nor-Sand: A simple critical state for sand." *Géotechnique*, 43(1), 91–103.

Lade, P. V. (1992). "Static instability and liquefaction of loose fine sandy slopes." *J. Geotech. Engrg.*, 10.1061/(ASCE)0733-9410(1992)118:1(51), 51–71.

Lade, P. V., Nelson, R. B., and Ito, Y. M. (1987). "Nonassociated flow and stability of granular materials." *J. Eng. Mech.*, 10.1061/(ASCE)0733-9399(1987)113:9(1302), 1302–1318.

Lade, P. V., Nelson, R. B., and Ito, Y. M. (1988). "Instability of granular materials with nonassociated flow." *J. Eng. Mech.*, 10.1061/(ASCE)0733-9399(1988)114:12(2173), 2173–2191.

Lade, P. V., and Pradel, D. (1990). "Instability and plastic flow of soils. I: Experimental observations." *J. Eng. Mech.*, 10.1061/(ASCE)0733-9399(1990)116:11(2532), 2532–2550.

Li, X. S., and Dafalias, Y. F. (2000). "Dilatancy for cohesionless soils." *Géotechnique*, 50(4), 449–460.

Li, X.-S., Dafalias, Y. F., and Wang, Z.-L. (1999). "State-dependent dilatancy in critical-state constitutive modeling of sand." *Can. Geotech. J.*, 36(4), 599–611.

Liu, J., Wang, G., Kamai, T., Zhang, F., Yang, J., and Shi, B. (2011). "Static liquefaction behavior of saturated fiber-reinforced sand in undrained ring-shear tests." *Geotext. Geomembr.*, 29(5), 462–471.

Lu, X., Huang, M., and Qian, J. (2011). "The onset of strain localization in cross-anisotropic soils under true triaxial condition." *Soils Found.*, 51(4), 693–700.

Manzari, M. T., and Dafalias, Y. F. (1997). "A critical state two-surface plasticity model for sands." *Géotechnique*, 47(2), 255–272.

Nova, R. (1994). "Controllability of the incremental response of soil specimens subjected to arbitrary loading programmes." *J. Mech. Behav. Mater.*, 5(2), 193–201.

Pietruszczak, S., and Stolle, D. F. E. (1987). "Deformation of strain softening material Part II: Modelling of strain softening response." *Comput. Geotech.*, 4(2), 109–123.

Prunier, F., Laouafa, F., Lignon, S., and Darve, F. (2009). "Bifurcation modeling in geomaterials: From the second-order work criterion to spectral analyses." *Int. J. Numer. Anal. Methods Geomech.*, 33(9), 1169–1202.

Rahman, M., Lo, S. R., and Baki, A. L. (2011). "Equivalent granular state parameter and undrained behaviour of sand–fines mixtures." *Acta Geotech.*, 6(4), 183–194.

Richart, F. E., Jr., Hall, J. R., Jr., and Woods, R. D. (1970). *Vibrations of soils and foundations*, Prentice-Hall, Englewood Cliffs, NJ.

Rudnicki, J. W., and Rice, J. R. (1975). "Conditions for the localization of the deformation in pressure-sensitive dilatant materials." *J. Mech. Phys. Solids*, 23(6), 371–394.

Sladen, J. A., D'Hollander, R. D., and Krahn, J. (1985). "The liquefaction of sands, a collapse surface approach." *Can. Geotech. J.*, 22(4), 564–578.

Valanis, K. C. (1985). "On the uniqueness of solution of the initial value problem in softening materials." *J. Appl. Mech.*, 52(3), 649–653.

Wan, R. G., and Guo, P. J. (2004). "Stress dilatancy and fabric dependencies on sand behavior." *J. Eng. Mech.*, 10.1061/(ASCE)0733-9399(2004)130:6(635), 635–645.

Wanatowski, D., and Chu, J. (2012). "Factors affecting pre-failure instability of sand under plane-strain conditions." *Géotechnique*, 62(2), 121–135.

Wood, M. D., and Belkheir, K. (1994). "Strain softening and state parameter for sand modeling." *Géotechnique*, 44(2), 335–339.

Yamamuro, J. A., and Lade, P. V. (1997). "Static liquefaction of very loose sands." *Can. Geotech. J.*, 34(6), 905–917.

Yang, J. (2002). "Non-uniqueness of flow liquefaction line for loose sand." *Géotechnique*, 52(10), 757–760.

Yang, J., and Li, X. S. (2004). "State-dependent strength of sands from the perspective of unified modeling." *J. Geotech. Geoenviron. Eng.*, 10.1061/(ASCE)1090-0241(2004)130:2(186), 186–198.